



# Refining the reaction mechanism of O<sub>2</sub> towards its co-substrate in cofactor-free dioxygenases

Pedro J. Silva

FP-ENAS/Fac. de Ciências da Saúde, Universidade Fernando Pessoa, Porto, Portugal

## ABSTRACT

Cofactor-less oxygenases perform challenging catalytic reactions between singlet co-substrates and triplet oxygen, in spite of apparently violating the spin-conservation rule. In 1-*H*-3-hydroxy-4-oxoquinaldine-2,4-dioxygenase, the active site has been suggested by quantum chemical computations to fine tune triplet oxygen reactivity, allowing it to interact rapidly with its singlet substrate without the need for spin inversion, and in urate oxidase the reaction is thought to proceed through electron transfer from the deprotonated substrate to an aminoacid sidechain, which then feeds the electron to the oxygen molecule. In this work, we perform additional quantum chemical computations on these two systems to elucidate several intriguing features unaddressed by previous workers. These computations establish that in both enzymes the reaction proceeds through direct electron transfer from co-substrate to O<sub>2</sub> followed by radical recombination, instead of minimum-energy crossing points between singlet and triplet potential energy surfaces without formal electron transfer. The active site does not affect the reactivity of oxygen directly but is crucial for the generation of the deprotonated form of the co-substrates, which have redox potentials far below those of their protonated forms and therefore may transfer electrons to oxygen without sizeable thermodynamic barriers. This mechanism seems to be shared by most cofactor-less oxidases studied so far.

**Subjects** Biochemistry

**Keywords** Computational chemistry, Minimum-energy crossing point, Oxygenase, Density-functional theory, Urate oxidase, Glutamate decarboxylase, Ring cleaving dioxygenase, DFT

## INTRODUCTION

Reactions where the number of unpaired electrons changes as reactants are transformed into products are not generally allowed by quantum mechanics due to Wigner's spin-conservation rule. This rule prevents the dioxygen molecule, which has two unpaired electrons and a  $S = 1$  (triplet) ground state, from easily reacting with acceptors in the singlet state ( $S = 0$ , like most organic molecules) to yield organic products without unpaired electrons. Such reactions are not, however, strictly impossible due to the intervention of spin-orbit coupling, which mixes both spin states. Understanding spin-forbidden reactions requires the characterization of the potential energy surfaces of the different spin-states involved in the reaction, and the location of the point where both surfaces touch each other (*Harvey, 2007; Harvey, 2014*). At this specific geometry (the "minimum-energy crossing point", henceforth abbreviated as MECP) the system

Submitted 20 June 2016  
Accepted 19 November 2016  
Published 20 December 2016

Corresponding author  
Pedro J. Silva, [pedros@ufp.edu.pt](mailto:pedros@ufp.edu.pt)

Academic editor  
Reinhard Schweitzer-Stenner

Additional Information and  
Declarations can be found on  
page 12

DOI 10.7717/peerj.2805

 Copyright  
2016 Silva

Distributed under  
Creative Commons CC-BY 4.0

**OPEN ACCESS**

may transition (or “hop”) between spin systems, with a probability which depends on the magnitude of the spin–orbit coupling and may be computed approximately according to the Landau–Zener equation (Nakamura, 1987). Since spin–orbit coupling is a relativistic effect which increases with the nuclear charge, formally spin–forbidden reactions become progressively easier as one descends down the periodic table, to the point that “spin–forbidden” transitions involving Ni, Cu or elements of the 5th (or lower) periods are as probable as “spin–allowed” transitions (Marian, 2001). Proteins which generate, use or transport dioxygen therefore usually rely on transition metals such as manganese, copper and iron (Ferguson-Miller & Babcock, 1996; Que & Ho, 1996; Sono et al., 1996; Wallar & Lipscomb, 1996; Yachandra, Sauer & Klein, 1996). A large class of enzymes devoid of metals (the flavoproteins) circumvents the problem with the help of flavin, which readily transfers one electron to oxygen yielding a separated radical pair consisting of a superoxide anion and a flavin-based radical (Massey, 1994; Mattevi, 2006). This mechanistical proposal has found experimental support from the observation of superoxide leakage to the reaction medium from the reaction of protein-bound flavins with dissolved oxygen (Massey et al., 1969; Boubacar et al., 2007; Daithankar et al., 2012) and spectroscopic identification of the flavin semiquinone radical in glycolate oxidase (Pennati & Gadda, 2011). A fast “flip” of the spin in the superoxide anion facilitated by strong spin–orbit coupling in the superoxide anion ( $-160\text{ cm}^{-1}$  (Huber & Herzberg, 2016)) then brings the pair to the singlet state, enabling straightforward, non-spin-forbidden reactivity. The reaction then proceeds through radical recombination (yielding a hydroperoxyflavin with no unpaired electrons, in monooxygenases (Mattevi, 2006; Visitsathawong et al., 2015)) or transfer of a second electron from the flavin semiquinone to superoxide, yielding hydrogen peroxide (Mattevi, 2006).

Several enzymes catalyze the addition of oxygen to suitably  $\pi$ -conjugated substrates in spite of lacking flavin or metals in their active sites, often through “substrate-assisted catalysis” (Fetzner & Steiner, 2010) which takes advantage of the enhanced reactivity of these conjugated system upon enzyme-promoted substrate deprotonation. Extensive computational details of the reaction mechanisms of coproporphyrinogen oxidase (Silva & Ramos, 2008) and vitamin K-dependent glutamate carboxylase (Silva & Ramos, 2007) confirmed that substrate deprotonation is indeed required for their catalytic action. Evidence for substrate deprotonation is also available for urate oxidase (Bui et al., 2014), although in this instance a more complex mechanism involving transient protein-based free radicals was proposed to be operative, based on EPR measurements of anaerobic preparations of substrate-bound enzyme (Gabison et al., 2011). Based on the reaction profile towards a superoxide-scavenging spin probe, radical-pair reactivity towards  $\text{O}_2$  has also been suggested to occur (Thierbach et al., 2014) in a bacterial ring-cleaving 2,4-dioxygenase active towards (1*H*)-3-hydroxy-4-oxoquinolines (EC 1.13.11.47), but recent computational results have been interpreted as contradicting this hypothesis, as the computed reaction energy for the electron transfer from substrate to  $\text{O}_2$  (8–11 kcal mol<sup>-1</sup>) would imply an “endothermic process [...] unlikely to happen spontaneously in the protein or in solvent” (Hernández-Ortega et al., 2015). As an alternative, these workers computed the energetics of a pathway (Fig. 1) consisting of addition of triplet oxygen

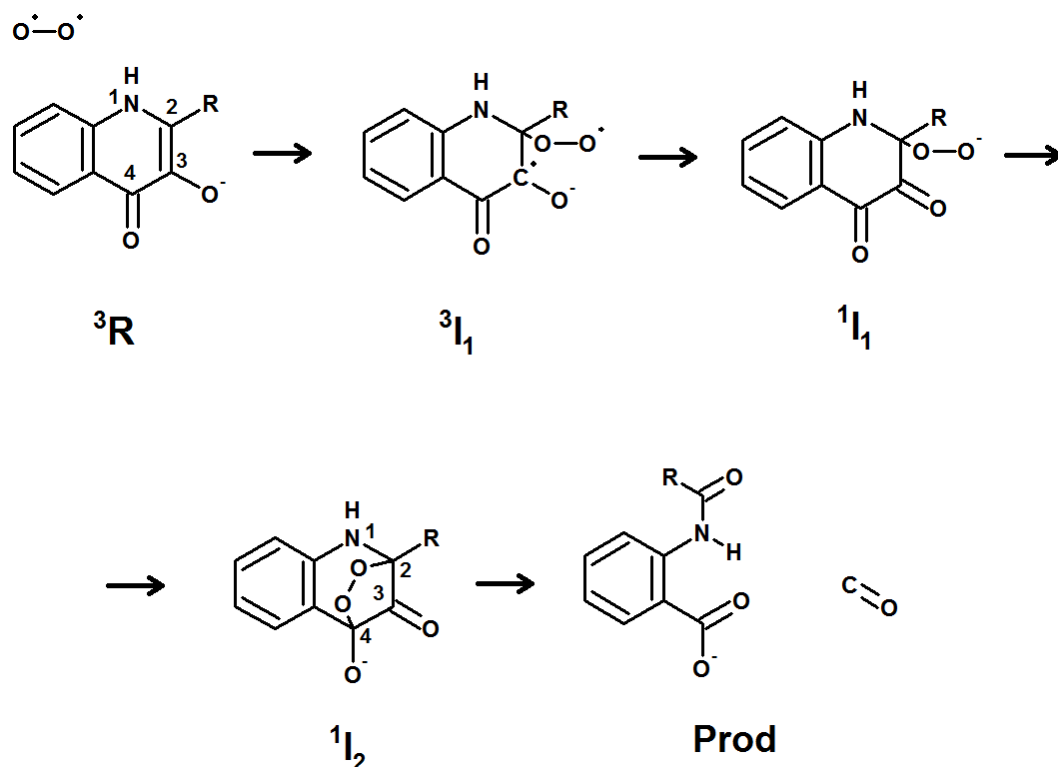


**Figure 1** Proposed mechanism for the reaction catalyzed by 1-H-3-hydroxy-4-oxoquinaldine-2,4-dioxygenase.

to the deprotonated substrate (yielding a triplet peroxide,  ${}^3\text{I}_1$ , 17 kcal mol<sup>-1</sup> above the reactants), followed by a transition to a singlet peroxide state ( ${}^1\text{I}_1$ , 8 kcal mol<sup>-1</sup> below the triplet state, i.e., 9 kcal mol<sup>-1</sup> above the reactant state). Minimum-energy crossing points between the singlet and triplet potential energy surfaces were not located in that work, but were predicted to lie around 10 kcal mol<sup>-1</sup> above the reactant state.

Some of the conclusions of the computational work of Hernández-Ortega et al. seem problematic: on the one hand, the computed 8–11 kcal mol<sup>-1</sup> endothermicity of the electron-transfer process from substrate to triplet oxygen does not seem enough to discard the possibility of an electron-transfer mechanism, since larger activation free energies of 17.4 kcal mol<sup>-1</sup> are able, according to transition state theory, of sustaining reaction rates of 1 s<sup>-1</sup> at room temperature; and on the other hand, the lack of data on the relative energies of the excited singlet state of the triplet peroxide intermediate and of the triplet state of the singlet peroxide intermediate leave open the possibility that those two potential energy surfaces do not cross between  ${}^3\text{I}_1$  and  ${}^1\text{I}_1$ , and that the minimum-energy crossing point actually lies between the reactant state ( ${}^3\text{R}$ ) and the singlet intermediate  ${}^1\text{I}_1$ , thereby completely bypassing the putative triplet peroxide ( ${}^3\text{I}_1$ ). In this work we perform additional computational studies of the putative intermediates of this reaction and conclude that the triplet peroxide state is never formed: the reaction instead proceeds directly from  ${}^3\text{R}$  to  ${}^1\text{I}_1$  either through low-lying minimum-energy crossing points or, most likely, through direct electron-transfer from substrate to oxygen, yielding a separated radical pair. Additional

computations in model systems for other reactions catalyzed by cofactor-less oxygenases strongly suggest that formation of such radical pairs should be the norm for inductively activated  $\pi$ -conjugated substrates.

## COMPUTATIONAL METHODS

Quantum chemical computations were performed with the Firefly ([Granovsky, 2013](#)) quantum chemistry package, which is partially based on the GAMESS (US) ([Schmidt et al., 1993](#)) source code. As in the original work ([Hernández-Ortega et al., 2015](#)), all computations were performed with the B3LYP density-functional ([Lee, Yang & Parr, 1988](#); [Becke, 1993](#); [Hertwig & Koch, 1995](#)). Optimized geometries of large models of intermediates  $^3R$ ,  $^3I_1$  and  $^1I_1$  were obtained from the Supporting information of [Hernández-Ortega et al. \(2015\)](#). Solution energies ([Tomasi & Persico, 1994](#); [Mennucci & Tomasi, 1997](#); [Cossi et al., 1998](#)) in water ( $\epsilon = 78.34$ ) and chlorobenzene ( $\epsilon = 5.7$ , mimicking the less polar environment of the protein active site) of the singlet and triplet states of these molecules were computed using the 6-31G(d,p) basis set complemented with diffuse functions on the oxygen atoms to allow a better description of the oxygen-based anionic species (henceforth referred to as basis set BS1).

Due to computational limitations, the search of minimum energy crossing points (MECP) between non-interacting singlet and triplet states required extensive trimming of the reaction model, which was reduced to the substrate, a water molecule, and the sidechains of the active-site dyad His<sub>251</sub>/Asp<sub>126</sub> responsible for substrate deprotonation. MECP were located employing the methodology developed by [Harvey et al. \(1998\)](#) at the B3LYP/BS1 level. Since MECP optimization in gas phase yield very different geometries from continuum MECP optimizations ([Silva & Ramos, 2007](#)), we performed this search with a PCM continuum model using water as the solvent. The C <sub>$\beta$</sub>  atoms of His<sub>251</sub> and Asp<sub>126</sub> were kept frozen to limit system flexibility to that possible in the enzyme active site. Investigation of CO release step were performed with the larger model suggested by Aitor-Hernández et al. (including the sidechains of His<sub>38</sub>, His<sub>100</sub>, Ser<sub>101</sub>, His<sub>102</sub>, Asp<sub>126</sub>, Trp<sub>160</sub>, His<sub>251</sub>, and the backbone amide linking Trp<sub>36</sub> to Cys<sub>37</sub>), with several atoms kept fixed to prevent unrealistic movements. The fixed atoms were: C <sub>$\beta$</sub>  of His<sub>100</sub> and His<sub>102</sub>, C <sub>$\alpha$</sub>  of Ser<sub>101</sub>, Trp<sub>36</sub> and Cys<sub>37</sub>, C <sub>$\beta$</sub>  and C <sub>$\gamma$</sub>  of His<sub>38</sub>, His<sub>251</sub> and Trp<sub>160</sub> and C <sub>$\alpha$</sub>  and C <sub>$\beta$</sub>  of Asp<sub>126</sub>. Very fine two-dimensional scans of the potential energy surface at the B3LYP/6-31G(d) level were performed by simultaneously varying the C<sub>3</sub>–C<sub>4</sub> and the O–O distances (while keeping the C<sub>2</sub>–C<sub>3</sub> distance fixed to prevent hysteresis). While the size of the system prevented the numerical computation (and updating) of the Hessians needed for saddle point optimization, this scanning procedure allowed the generation of smooth potential energy surfaces which enabled the location of high quality transition structure guesses.

The activation energy of the one-electron transfer between substrates and O<sub>2</sub> were estimated by applying Marcus theory for electron transfer, as suggested by [Blomberg & Siegbahn \(2003\)](#) and subsequently modified by [Silva & Ramos \(2008\)](#). As in previous works by our and other groups ([Silva & Ramos, 2008](#); [Silva & Ramos, 2009](#); [Silva, 2014](#); [Wijaya et al., 2016](#)) reorganization energies for every molecule in both oxidation states

**Table 1** Comparison of the quality of the energies obtained with the truncated model (which includes only the substrate and the Asp/His dyad) vs. the energies obtained with the large model used by *Hernandez-Ortega et al. (2015)*. All energies are computed vs. the respective reactant state at the B3LYP/BS1 theory level in water. The large model includes the sidechains of His38, His100, Ser101, His102, Asp126, Trp160, His251, and the backbone amide linking Trp36 to Cys37. All coordinates were taken from the Supporting information of *Hernandez-Ortega et al. (2015)* and used without further optimization.

Quinoline substituent	Model used	$^3I_1$	$^1I_1$
-F	Large model	5.5	-10.1
-F	His <sub>251</sub> /Asp <sub>126</sub> + substrate	5.3	-10.1
-CH <sub>3</sub>	Large model	12.6	0.6
-CH <sub>3</sub>	His <sub>251</sub> /Asp <sub>126</sub> + substrate	13.5	1.2
-(CH <sub>2</sub> ) <sub>4</sub> CH <sub>3</sub>	Large model	19.2	4.8
-(CH <sub>2</sub> ) <sub>4</sub> CH <sub>3</sub>	His <sub>251</sub> /Asp <sub>126</sub> + substrate	18.7	1.5
-NO <sub>2</sub>	Large model	19.0	7.2
-NO <sub>2</sub>	His <sub>251</sub> /Asp <sub>126</sub> + substrate	24.0	10.6

were computed using the water-optimized reactant geometries for the product state (and vice-versa) and activation energies were then computed by building appropriate Marcus parabolas using these reorganization energies. The smaller size of these models allowed us to increase the size of the basis set in these computations to 6-311G(d,p), while keeping the diffuse functions on the oxygen atoms to allow a better description of the oxygen-based anionic species (henceforth this basis set will be referred to as BS2). Atomic charge and spin density distributions were calculated with a Mulliken population analysis (*Mulliken, 1955*) based on symmetrically orthogonalized orbitals (*Löwdin, 1970*).

Computation of the binding modes of 2-methyl- and 2-butyl-(1*H*)-3-hydroxy-4-oxoquinoline towards 2,4-dioxygenase (PDB:2WJ4 (*Steiner et al., 2010*)) were performed in YASARA Structure (*Krieger & Vriend, 2014*) using its AutoDock VINA module with default parameters (*Trott & Olson, 2010*). The docking region was confined to a 39.8 × 34.8 × 34.8 Å box centered on residues Trp36, His38, His100, Ser101, His102, Asp126, Trp160, and His251. Residues Gly35, Trp36, His38, His100, Ser101, His102, Leu128, Phe136, Leu156, Trp160, Met177, Trp185, Ile192 and His251 were kept flexible during the docking procedure.

## RESULTS AND DISCUSSION

### 1-*H*-3-hydroxy-4-oxoquinoline-2,4-dioxygenase

We started the search for minimum-energy crossing points between the triplet and singlet states of O<sub>2</sub> and deprotonated (1*H*)-3-hydroxy-4-oxoquinolines from the reported structures of the  $^3I_1$  intermediate. To keep the computations tractable most of the surrounding aminoacids were excised, and only the Asp-His dyad responsible for the initial deprotonation of substrate (*Steiner et al., 2010*; *Hernandez-Ortega et al., 2014*) and charge stabilization of the  $^3I_1/{}^1I_1$  intermediates was kept. **Table 1** shows that this truncation has very modest effects on the reaction energetics, and should therefore not introduce relevant errors.

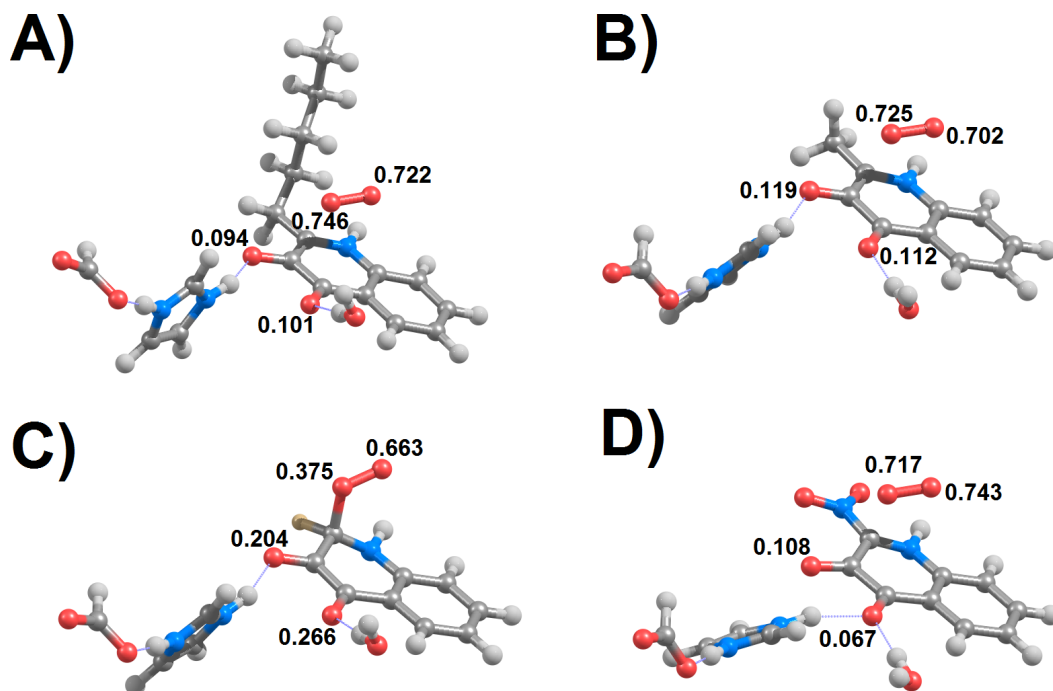


**Figure 2** Optimized B3LYP/BS1 geometries of the minimum-energy crossing points of (1H)-3-hydroxy-4-oxoquinolines bearing pentyl (A), methyl (B), fluoro (C) and nitro (D) substituents. Spins on the oxygen atoms are shown for the triplet state at each of these geometries.

As in previous work by *Hernandez-Ortega et al. (2014)*, all computations were repeated for four different (1H)-3-hydroxy-4-oxoquinolines to ascertain the influence of different substituents (methyl, pentyl, fluor and nitro) in the reaction course. The minimum-energy crossing points found (*Fig. 2*) were dramatically different from the  $^3I_1$  intermediates postulated in the previous work, which contain short (1.499–1.502 Å) substrate-oxygen bonds and longer O–O bonds (1.38 Å) than observed for free superoxide (1.334 Å). The sole exception was found to be the fluoro-substituted substrate, where the MECP geometry presented a short (1.56 Å) C–O distance (*Table 2*) and where the spin distribution at the triplet state (*Fig. 2*) was the most different from the initial reactant state. In spite of the large change relative to the initial state, the MECP for this substrate proved to be the most energetically accessible of all the tested quinolines (*Table 2*). Geometry optimizations of the triplet state starting from these MECP geometries invariably yielded the triplet reactant state and optimizations of the singlet state starting from this same geometry invariably collapsed into  $^1I_1$  intermediates. In contrast to the earlier workers, optimization of  $^3I_1$  intermediates proved to be impossible with HODMe or HODpentyl due to spontaneous break of the postulated substrate-O, yielding the original triplet reactant state. For HODF and HODNO<sub>2</sub> the  $^3I_1$  intermediates proved to be local minima in the potential energy surface, as found by Hernandez-Ortega et al., but the C–O bond in  $^3I_1$  HODF was found to be 0.1 Å longer than found by them. This behaviour was observed both in the Asp/His only model (6-31G(d,p)(+) with a PCM continuum) and in the full model (6-31G(d)(+) in gas phase). Surprisingly, gas-phase optimization of the full



**Table 2** Characterization of the minimum-energy crossing points between the singlet and triplet surfaces of oxygen:(1*H*)-3-hydroxy-4-oxoquinoline systems in the presence of the His<sub>251</sub>/Asp<sub>126</sub> catalytic dyad, at the B3LYP/BS1 level in a water continuum. The C<sub>β</sub> atoms of His251 and Asp126 were kept frozen to limit system flexibility to that possible in the enzyme active site. n.a: not applicable, as the <sup>3</sup>I<sub>1</sub> species for these substituents are not local minima in the potential energy surface and collapse into separated substrate and triplet O<sub>2</sub>. For the -NO<sub>2</sub> substituted quinoline, the substrate–oxygen distance in <sup>1</sup>I<sub>1</sub> is quite long (2.07 Å), and this intermediate is more properly described as a superoxide:substrate radical pair.

Quinoline substituent	-(CH <sub>2</sub> ) <sub>4</sub> CH <sub>3</sub>	-CH <sub>3</sub>	-F	-NO <sub>2</sub>
C–O distance (Å) at the MECP	2.308	2.23	1.568	1.968
O–O distance (Å) at the MECP	1.303	1.307	1.326	1.304
MECP energy (kcal mol <sup>-1</sup> ) vs. reactants	16.8	15.2	9.2	24.2
<sup>1</sup> I <sub>1</sub> energy (kcal mol <sup>-1</sup> ) vs. reactants	11.1	9.0	-3.4	23.6
<sup>3</sup> I <sub>1</sub> energy (kcal mol <sup>-1</sup> ) vs. reactants	n.a	n.a	6.9	25.4

system with 6-31G (as used by Hernandez-Ortega et al.) did not afford stable <sup>3</sup>I<sub>1</sub> with any substrate. I cannot tell whether the difference in results is due to subtle differences in the basis sets exponents, DFT integration grids, the particular solvation model used, to their choice of freezing all atoms in the active site aminoacids (vs. only a few backbone atoms in the present work) or to the particular choice of basis sets: the basis set they used for geometry optimizations (6-31G) lacks diffuse or polarization functions and is therefore less flexible/accurate than the 6-31G(d,p)(+) basis set I chose. The transition states leading from separated triplet reactants to these <sup>3</sup>I<sub>1</sub> intermediates lie less than 0.2 kcal mol<sup>-1</sup> above <sup>3</sup>I<sub>1</sub>, as also observed by Hernández-Ortega et al. The lack of minimum energy crossing points in the region of the potential energy surface leading from <sup>3</sup>I<sub>1</sub> to <sup>1</sup>I<sub>1</sub> geometries entails that the reaction will most likely proceed directly through the MECP and thence to <sup>1</sup>I<sub>1</sub> and that in the few cases where the <sup>3</sup>I<sub>1</sub> intermediates are stable their formation is an unproductive side-reaction in spite of their energetic accessibility (Table 2).

A preference for direct electron transfer to O<sub>2</sub> instead of a pathway relying on minimum-energy crossing points between surfaces of different spin multiplicity has been postulated before (e.g., Massey, 1994) for the flavin:O<sub>2</sub> system and confirmed by quantum chemical computations (Prabhakar et al., 2002). Such preference is not limited to flavins, and has also been confirmed computationally for the deprotonated pyrrole in the reaction catalyzed by the oxygen-dependent coproporphyrinogen oxidase (Silva & Ramos, 2008). For the present enzymatic system, Hernández-Ortega et al. found that electron transfer from substrate to O<sub>2</sub> was endergonic by 8–11 kcal mol<sup>-1</sup>, and concluded from these data (and from the inability of obtaining a converged wavefunction for the substrate radical:superoxide pair) that such a pathway would be impossible for this reaction. However, current SCF algorithms are well-known to have difficulties when attempting to enforce specific electron distributions (such as radical pairs lying at higher energies than the non-radical pair alternative), and therefore encountering convergence difficulties may not point to an intrinsic instability of those pairs but simply be a consequence of numerical/algorithmic difficulties. We have therefore analyzed the thermodynamic and kinetic feasibility of direct electron transfer from substituted quinolines to O<sub>2</sub> using a Marcus formalism (Table 3).

**Table 3** Reaction energies and activation energies of the electron-transfer from substituted (1*H*)-3-hydroxy-4-oxoquinolines to dioxygen, at the B3LYP/BS2//B3LYP/BS1 level, computed using Marcus theory for electron transfer. Unless otherwise noted, the 3-hydroxyl group remained in the deprotonated state. Substituents are shown ordered by increased values of their Hammett  $\sigma_m$  parameters (Hansch, Leo & Taft, 1991).

Quinoline substituent	In chlorobenzene		In water	
	Activation energy (kcal mol <sup>-1</sup> )	Reaction energy (kcal mol <sup>-1</sup> )	Activation energy (kcal mol <sup>-1</sup> )	Reaction energy (kcal mol <sup>-1</sup> )
-NH <sub>2</sub>	3.4	-1.5	2.0	-4.8
-COO <sup>-</sup>	1.5	-5.1	5.9	4.4
-(CH <sub>2</sub> ) <sub>4</sub> CH <sub>3</sub>	7.1	6.0	5.2	3.0
-CH <sub>3</sub>	6.8	5.5	4.9	2.5
-CH <sub>3</sub> (protonated quinoline)	86.2	58.1	46.9	38.7
-F	11.1	10.9	8.6	7.8
-COCH <sub>3</sub>	22.5	21.5	16.6	16.5
-CN	24.6	22.9	18.3	18.0
-NO	23.9	23.7	20.0	20.0
-NO <sub>2</sub>	41.2	33.1	31.1	27.5

This formalism relies on the separate computation of the energies of electron-donor and acceptor, but such reliance is not expected to significantly detract from the quality of the results, as optimization of the radical pairs at large separations (20–120 Å, to facilitate numerical convergence of the SCF procedure) yields energies which are very similar (within 0.5 kcal mol<sup>-1</sup> in the gas phase) to the sums of the individually optimized superoxide and substrate radical (<https://dx.doi.org/10.6084/m9.figshare.3426062.v22>). The reaction rate was found to be strongly correlated with the electron-donating capability of the quinoline substituent (Table 3). For electron-donating and weakly-withdrawing substituents the reaction rate can be extremely fast, regardless of the polarity of the solvent. Polar environments generally lower the activation energy of this electron-transfer, enabling it to occur at rates exceeding 0.1 s<sup>-1</sup> even for such electron-withdrawing substituents as acetyl, nitroso or nitrile. Overall, Table 3 shows that direct electron transfer from deprotonated co-substrate to O<sub>2</sub> is predicted to be fast and uncomplicated even when the co-substrate bears moderately deactivating substituents. Comparison of these activation energies to the energies of the minimum-energy crossing points (Table 2) shows that for HODMe and HODpentyl the direct electron transfer route is favored over the reaction paths containing MECP (or the <sup>3</sup>I<sub>1</sub> state found by Hernández-Ortega) by more than 8 kcal mol<sup>-1</sup>. The generation of the peroxide intermediate <sup>1</sup>I<sub>1</sub> is therefore most likely to proceed (in agreement with the proposal by Thierbach *et al.* (2014) and in contrast to the mechanism postulated by (Hernández-Ortega *et al.* (2015)) through electron transfer from substrate to O<sub>2</sub>, followed by recombination of the substrate-based radical with superoxide.

The endergonicity of the electron transfer step does not affect the viability of the process, since all it takes for a reaction to occur is that those endoenergetic steps are followed by sufficiently fast and exoenergetic steps so that the total activation barrier lies below *ca.*



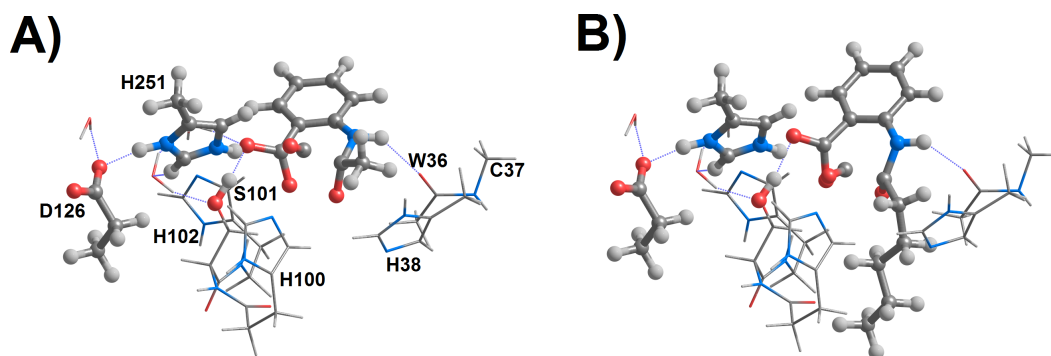


**Figure 3** Proposed geometries of the transition states for the  ${}^1\text{I}_2 \rightarrow$  product reaction step for the (A) methyl-, and (B) pentyl-substituted 4-oxoquinolines. Coordinates taken from the Supporting information of [Hernández-Ortega et al. \(2015\)](#). Trp160 has been omitted from images for clarity.

$20 \text{ kcal mol}^{-1}$  (i.e., reaction rates above  $10^{-2} \text{ s}^{-1}$ ) and the overall reaction has a negative  $\Delta G$  at the reactants/products concentrations present in the cell (so that the reaction proceeds in the direct rather than the reverse direction). In fact, superoxide formation has been experimentally confirmed in flavocytochrome *b2* ([Boubacar et al., 2007](#)), which contains a FMN with a redox potential of  $-45 \text{ mV}$  ([Capeillère-Blandin, Barber & Bray, 1986](#)) and from proline dehydrogenase ([White et al., 2007](#)), which harbors a FAD with a  $-75 \text{ mV}$  redox potential, in spite of the endergonicity of the electron transfer from these cofactors to  $\text{O}_2$  ( $E_{\text{m}}\text{O}_2/\text{O}_2^- = -330 \text{ mV}$ ).

Hernández-Ortega et al. have shown that the peroxide intermediate  ${}^1\text{I}_1$  quickly becomes an endoperoxide ( ${}^1\text{I}_2$ ) through attack of the substrate  $\text{C}_4$  by the terminal oxygen. Release of  $\text{C}=\text{O}$  from  ${}^1\text{I}_2$  yields a carboxylate function on  $\text{C}_4$  and occurs quickly due to the stabilization of the nascent negative charge by hydrogen bonding with Ser101 ( $1.51 \text{ \AA}$ ) and strong interaction with the positively-charged His251 ( $2.16 \text{ \AA}$ ). In their computational investigation of this reaction step with quinolines bearing the much longer pentyl substituent, these researchers observed a remarkable increase of the activation energy for CO release of almost  $16 \text{ kcal mol}^{-1}$ . Inspection of the structure of the transition state of the transformation of  ${}^1\text{I}_2$  into products reveals that the high activation energy of the pentyl-substituted quinoline is due to the use of the same binding mode for this quinoline as for the methyl-substituted quinoline, which introduces steric clashes between the pentyl-group and His38, His100 and the Trp36-Cys37 backbone. To avoid these clashes, the pentyl-substituted substrate is forced to rotate  $30^\circ$  around the axis perpendicular to the quinoline ring, thus increasing the separation between the substrate and Ser101 (to  $1.85 \text{ \AA}$ ) and His251 (to  $2.67 \text{ \AA}$ ), and strongly decreasing the charge stabilization provided by these residues on the nascent carboxylate ([Fig. 3](#)).

Although the  $16 \text{ kcal mol}^{-1}$  increase of activation energy for the CO release step in the pentyl-substituted was regarded by the original researchers ([Hernández-Ortega et al., 2015](#)) as “in agreement with the drop in [experimental] rate constant” reported earlier in the same paper for the butyl-substituted substrate, the observed 30% increase in  $k_{\text{cat}}$  and 10-fold decrease of  $k_{\text{cat}}/K_{\text{M}}$  are not consistent with the 12 orders of magnitude

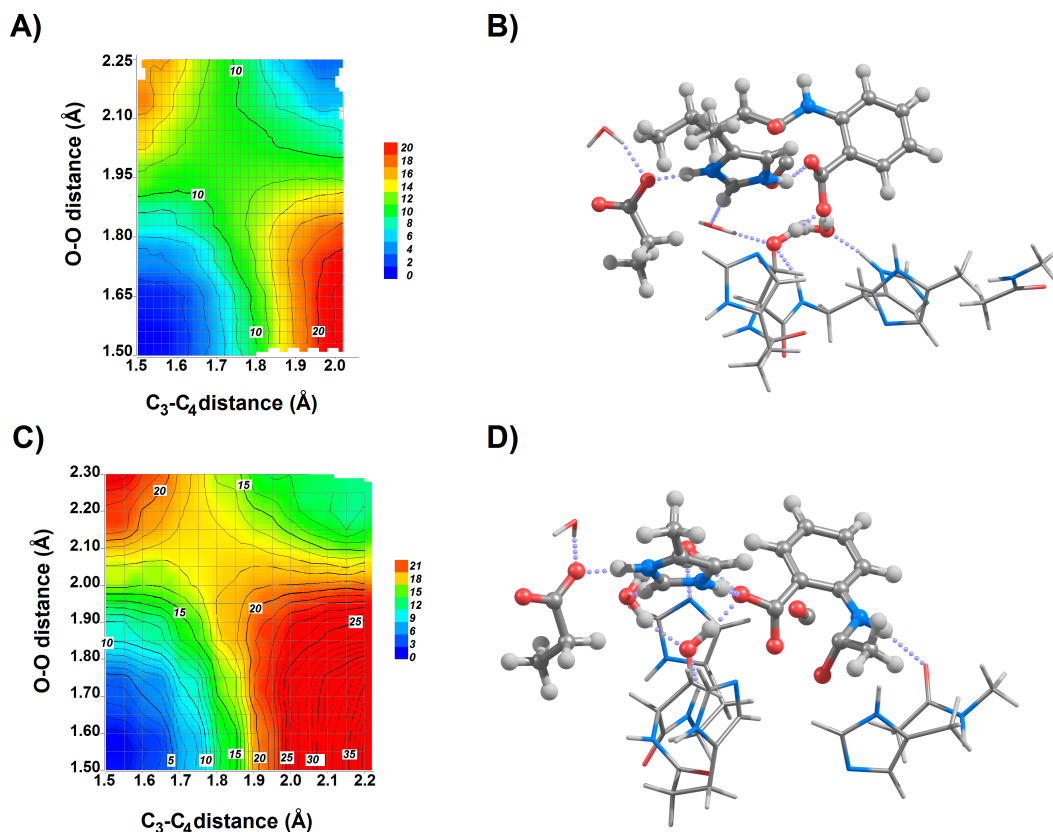


**Figure 4** Newly-derived potential energy surfaces (at the B3LYP/6-31G(d) theory level) of the  $^1\text{I}_2 \rightarrow$  product reaction step for the (A) butyl-, and (C) methyl-substituted 4-oxoquinolines. Geometries of the transition states for the  $^1\text{I}_2 \rightarrow$  product reaction step for the (B) butyl-, and (D) methyl-substituted 4-oxoquinolines are shown, with the substrate and sidechains of Ser101, Asp126 and His251 highlighted. Trp160 has been omitted from the images for clarity.

difference in  $k_{\text{cat}}$  expected from such a difference in activation energy. Additional evidence against the mechanistic relevance of the proposed binding mode for the pentyl-substituted substrate comes from the superposition of the transition state model coordinates with the crystallographic structure of the enzyme: even after this  $30^\circ$  rotation, the proposed position of pentyl group lies on the space occupied by the Pro35-Gly36 stretch of the enzyme, which had been left out of the active site model. Long hydrocarbon substituents may, however, be accommodated if a binding mode rotated by  $240^\circ$  is assumed, which places the aliphatic chain in the entrance channel bordered by Leu128, Phe136, Leu165, Val159, Trp160, Gln221 and His251. This binding mode was confirmed as the best hit in docking computations using Autodock VINA. A subsequent two-dimensional scan of the coordinates involved in the  $^1\text{I}_2 \rightarrow$  product transition showed that in this binding mode a very low energy pathway for CO release is accessible through a transition structure stabilized through interactions with Ser101 and His251 (Fig. 4B and Table 4). An identical scan was performed for the methyl-substituted quinolone in the original orientation (Table 4, Figs. 4C and 4D). The small differences in activation energies between both 4-oxoquinolines

**Table 4** Comparison of the transition states of the CO release step for methyl- and butyl-substituted quinolones.

	Butyl quinoline <sup>a</sup>	Methyl quinoline <sup>a</sup>	Methyl quinoline <sup>b</sup>
C <sub>3</sub> –C <sub>2</sub> distance (Å)	1.71	1.77	1.749
O–O distance (Å)	1.99	2.09	2.055
TS energy vs. <sup>1</sup> I <sub>2</sub> (kcal mol <sup>-1</sup> ) in water	8.1	11.3	8.0
TS energy vs. <sup>1</sup> I <sub>2</sub> (kcal mol <sup>-1</sup> ) ( $\epsilon = 5.7$ )	8.0	11.4	8.4
Ser101–O <sub>4</sub> distance (Å)	1.57	1.58	1.741
His251–O distance (Å)	1.89	1.83	Not applicable

**Notes.**

<sup>a</sup>Structure obtained from very fine 2D-scans, with an active site model including the sidechains of His38, His100, Ser101, His102, Asp126, Trp160, His251, and the backbone of Trp36.

<sup>b</sup>Structure obtained from a complete saddle-point optimization in a minimal model including only the substrate, a water molecule and a methanol molecule mimicking Ser101.

Energies were computed at the B3LYP/BS2 level and do not include zero-point vibrational effects.

**Table 5** Reaction energies and activation energies of the electron-transfer from urate dianion to dioxygen or aminoacid sidechains, at the B3LYP/BS2//B3LYP/BS1 level.

Electron acceptor	In chlorobenzene		In water	
	Activation energy (kcal mol <sup>-1</sup> )	Reaction energy (kcal mol <sup>-1</sup> )	Activation energy (kcal mol <sup>-1</sup> )	Reaction energy (kcal mol <sup>-1</sup> )
O <sub>2</sub>	0.8	–9.3	4.2	0.1
His <sup>+</sup>	18.8	17.0	48.1	47.5
Lys <sup>+</sup>	34.3	30.9	65.2	64.3
Arg <sup>+</sup>	24.5	20.5	51.5	51.4

are fully consistent with the lack of dramatic differences in the experimentally-measured kinetic parameters.

### Other oxygenases

The experimental observation of EPR radical signals in anaerobic urate oxidase preparations upon incubation with uric acid (*Gabison et al., 2011*) is thought to support a reaction mechanism where urate dianion (generated through deprotonation of uric acid at the enzyme active site) transfers an electron to aminoacid sidechains (Lys, Arg or His) and reaction with O<sub>2</sub> occurs through electron transfer from these aminoacid radicals. Our DFT computations ([Table 5](#)) show that direct electron from the urate dianion to O<sub>2</sub> has such a low activation energy that no electron transfer to an active site aminoacid needs to occur to enable catalysis, and no minimum-energy crossing point between the singlet and triplet surfaces needs to be reached. The radical observed anaerobically (which may be His-based) should therefore play no role in the catalytic mechanism.

Finally, we computed the activation energy for the electron transfer between vitamin K and O<sub>2</sub>. The value obtained (5.3 kcal mol<sup>-1</sup> in chlorobenzene, 3.3 kcal mol<sup>-1</sup> in water) is, again, inferior to the energy of the minimum-energy crossing point between the singlet and triplet surfaces (15.3 kcal mol<sup>-1</sup> in water (*Silva & Ramos, 2007*)). It thus appears that for all cofactor-less oxidases studied computationally so far (urate oxidase, 1-*H*-3-hydroxy-4-oxoquinoline-2,4-dioxygenase, coproporphyrinogen oxidase and vitamin K-dependent

glutamate carboxylase) catalysis occurs through direct electron transfer from substrate to O<sub>2</sub> followed by radical recombination, instead of minimum-energy crossing points without formal electron transfer. A novel nogalamycin monooxygenase (*Machovina, Usselman & DuBois, 2016*) has recently been shown experimentally to also follow this paradigm, which thus appears to be the most general strategy for the enzyme-catalyzed reaction of triplet O<sub>2</sub> with conjugated organic substrates in the absence of metal cofactors.

## CONCLUSIONS

The computations described in this paper show that the previously postulated triplet endoperoxide intermediate (<sup>3</sup>I<sub>1</sub>) is most unlikely to play a role in the reaction mechanism of bacterial ring-cleaving 2,4-dioxygenase, as the minimum energy crossing point between the singlet and triplet surfaces directly connects the reactants to the singlet endoperoxide intermediate (<sup>1</sup>I<sub>1</sub>), and no MECP connecting the putative <sup>3</sup>I<sub>1</sub> intermediate to <sup>1</sup>I<sub>1</sub> is present. Moreover, the computed activation energy for the direct electron transfer from substrate to O<sub>2</sub> is lower than the MECP energy for substrates bearing electron-donating or weak electron-withdrawing groups at the 2- position, enabling the formation of separated radical pairs after the 3-hydroxy group in the substrate is suitably deprotonated by the His251/Asp126 dyad ([Table 2](#)). Similar separated radical pairs also appear as the most likely intermediates in all other cofactor-less oxygenases studied computationally so far. The computation of small activation energies (comparable to those measured experimentally) using small models which do not take into account the full complexity of the active site/protein environment nor interact directly with the attacking dioxygen molecule strongly suggests that the additional complexity of the protein environment is not needed to “enhance the reactivity” of O<sub>2</sub> *per se*, but simply to ensure that the substrates approach the critical portion of the active site (the Asp/His dyad responsible for the initial deprotonation) in the proper orientation. Finally, 1-*H*-3-hydroxy-4-oxoquinaldine-2,4-dioxygenase reactivity towards substrates bearing long alkyl chains on the 2-position is not possible in the originally postulated binding mode: the enzyme instead relies on a different binding mode which enables catalysis of the CO release step by positioning the nascent negative charges in a suitably stabilizing environment and affords reaction rates similar to those obtained with the sterically unencumbered HODMe substrate.

## ADDITIONAL INFORMATION AND DECLARATIONS

### Funding

The author received no funding for this work, which was performed using computational resources acquired under a previous project (PTDC/QUI-QUI/111288/2009) financed by FEDER through Programa Operacional Factores de Competitividade–COMPETE and by Portuguese Funds through FCT–Fundação para a Ciência e a Tecnologia. The FP-ENAS Research Unit further receives some support from additional Portuguese Funds through a grant from FCT–Fundação para a Ciência e a Tecnologia (UID/Multi/04546/2013). The

fundere had no role in study design, data collection and analysis, decision to publish, or preparation of the manuscript.

### Grant Disclosures

The following grant information was disclosed by the author:

FEDER through Programa Operacional Factores de Competitividade–COMPETE.

FCT–Fundação para a Ciência e a Tecnologia: UID/Multi/04546/2013.

### Competing Interests

Pedro J. Silva is an Academic Editor for PeerJ. The author does not have any other competing interests.

### Author Contributions

- Pedro J. Silva conceived and designed the experiments, performed the experiments, analyzed the data, wrote the paper, prepared figures and/or tables.

### Data Availability

The following information was supplied regarding data availability:

Silva, Pedro (2016): Refining the reaction mechanism of O<sub>2</sub> towards its substrate in cofactor-free dioxygenases. Figshare. <https://dx.doi.org/10.6084/m9.figshare.3426062.v22>.

### Supplemental Information

Supplemental information for this article can be found online at <http://dx.doi.org/10.7717/peerj.2805#supplemental-information>.

## REFERENCES

- Becke AD.** 1993. Density-functional thermochemistry. III. The role of exact exchange. *The Journal of Chemical Physics* **98**:5648–5652 DOI [10.1063/1.464913](https://doi.org/10.1063/1.464913).
- Blomberg MRA, Siegbahn PEM.** 2003. A quantum chemical study of tyrosyl reduction and O—O bond formation in photosystem II. *Molecular Physics* **101**:323–333.
- Boubacar AKO, Pethe S, Mahy J-P, Lederer F.** 2007. Flavocytochrome b<sub>2</sub>: reactivity of its flavin with molecular oxygen. *Biochemistry* **46**:13080–13088 DOI [10.1021/bi7013757](https://doi.org/10.1021/bi7013757).
- Bui S, Von Stetten D, Jambrina PG, Prangé T, Colloc'h N, De Sanctis D, Royant A, Rosta E, Steiner RA.** 2014. Direct evidence for a peroxide intermediate and a reactive enzyme-substrate-dioxygen configuration in a cofactor-free oxidase. *Angewandte Chemie International Edition* **53**:13710–13714 DOI [10.1002/anie.201405485](https://doi.org/10.1002/anie.201405485).
- Capeillère-Blandin C, Barber MJ, Bray RC.** 1986. Comparison of the processes involved in reduction by the substrate for two homologous flavocytochromes b<sub>2</sub> from different species of yeast. *The Biochemical Journal* **238**:745–756 DOI [10.1042/bj2380745](https://doi.org/10.1042/bj2380745).
- Cossi M, Mennucci B, Pitarch J, Tomasi J.** 1998. Correction of cavity-induced errors in polarization charges of continuum solvation models. *Journal of Computational Chemistry* **19**:833–846 DOI [10.1002/\(SICI\)1096-987X\(199806\)19:8<833::AID-JCC3>3.0.CO;2-Q](https://doi.org/10.1002/(SICI)1096-987X(199806)19:8<833::AID-JCC3>3.0.CO;2-Q).

- Daithankar VN, Wang W, Trujillo JR, Thorpe C. 2012.** Flavin-linked Erv-family sulfhydryl oxidases release superoxide anion during catalytic turnover. *Biochemistry* **51**:265–272 DOI [10.1021/bi201672h](https://doi.org/10.1021/bi201672h).
- Ferguson-Miller S, Babcock GT. 1996.** Heme/copper terminal oxidases. *Chemical Reviews* **96**:2889–2908 DOI [10.1021/cr950051s](https://doi.org/10.1021/cr950051s).
- Fetzner S, Steiner RA. 2010.** Cofactor-independent oxidases and oxygenases. *Applied Microbiology and Biotechnology* **86**:791–804 DOI [10.1007/s00253-010-2455-0](https://doi.org/10.1007/s00253-010-2455-0).
- Gabison L, Chopard C, Colloch N, Peyrot F, Castro B, El Hajji M, Altarsha M, Monard G, Chiadmi M, Prangé T. 2011.** X-ray, ESR, and quantum mechanics studies unravel a spin well in the cofactor-less urate oxidase. *Proteins: Structure, Function, and Bioinformatics* **79**:1964–1976 DOI [10.1002/prot.23022](https://doi.org/10.1002/prot.23022).
- Granovsky AA. 2013.** Firefly 8.0.0. Available at <http://classic.chem.msu.su/gran/firefly/index.html>.
- Hansch C, Leo A, Taft RW. 1991.** A survey of hammett substituent constants and resonance and field parameters. *Chemical Reviews* **91**:165–195 DOI [10.1021/cr00002a004](https://doi.org/10.1021/cr00002a004).
- Harvey JN. 2007.** Understanding the kinetics of spin-forbidden chemical reactions. *Physical Chemistry Chemical Physics* **9**:331–343 DOI [10.1039/B614390C](https://doi.org/10.1039/B614390C).
- Harvey JN. 2014.** Spin-forbidden reactions: computational insight into mechanisms and kinetics. *Wiley Interdisciplinary Reviews: Computational Molecular Science* **4**:1–14.
- Harvey JN, Aschi M, Schwarz H, Koch W. 1998.** The singlet and triplet states of phenyl cation. A hybrid approach for locating minimum energy crossing points between non-interacting potential energy surfaces. *Theoretical Chemistry Accounts: Theory, Computation, and Modeling* **99**:95–99 DOI [10.1007/s002140050309](https://doi.org/10.1007/s002140050309).
- Hernandez-Ortega A, Quesne MG, Bui S, Heuts DPHM, Steiner RA, Heyes DJ, De Visser SP, Scrutton NS. 2014.** Origin of the proton-transfer step in the cofactor-free (1H)-3-hydroxy-4-oxoquinaldine 2,4-dioxygenase: effect of the basicity of an active site his residue. *Journal of Biological Chemistry* **289**:8620–8632 DOI [10.1074/jbc.M113.543033](https://doi.org/10.1074/jbc.M113.543033).
- Hernández-Ortega A, Quesne MG, Bui S, Heyes DJ, Steiner RA, Scrutton NS, De Visser SP. 2015.** Catalytic mechanism of cofactor-free dioxygenases and how they circumvent spin-forbidden oxygenation of their substrates. *Journal of the American Chemical Society* **137**:7474–7487 DOI [10.1021/jacs.5b03836](https://doi.org/10.1021/jacs.5b03836).
- Hertwig RH, Koch W. 1995.** On the accuracy of density functionals and their basis set dependence: an extensive study on the main group homonuclear diatomic molecules Li<sub>2</sub> to Br<sub>2</sub>. *Journal of Computational Chemistry* **16**:576–585 DOI [10.1002/jcc.540160506](https://doi.org/10.1002/jcc.540160506).
- Huber KP, Herzberg G. 2016.** Constants of diatomic molecules. In: Linstrom PJ, Mallard WG, eds. *NIST chemistry WebBook, NIST standard reference database number 69*. Gaithersburg: National Institute of Standards and Technology.
- Krieger E, Vriend G. 2014.** YASARA View—molecular graphics for all devices—from smartphones to workstations. *Bioinformatics* **30**:2981–2982 DOI [10.1093/bioinformatics/btu426](https://doi.org/10.1093/bioinformatics/btu426).



- Lee C, Yang W, Parr RG. 1988. Development of the Colle-Salvetti correlation-energy formula into a functional of the electron density. *Physical Review B* 37:785–789 DOI 10.1103/PhysRevB.37.785.
- Löwdin P-O. 1970. On the nonorthogonality problem. In: *Advances in quantum chemistry*. Vol. 5, Academic Press: 185–199.
- Machovina MM, Usselman RJ, DuBois JL. 2016. Monooxygenase substrates mimic flavin to catalyze cofactorless oxygenations. *Journal of Biological Chemistry* 291:17816–17828 DOI 10.1074/jbc.M116.730051.
- Marian C. 2001. Spin-orbit coupling in molecules. *Reviews in Computational Chemistry* 17:99–204 DOI 10.1002/0471224413.ch3.
- Massey V. 1994. Activation of molecular oxygen by flavins and flavoproteins. *The Journal of Biological Chemistry* 269:22459–22462.
- Massey V, Strickland S, Mayhew SG, Howell LG, Engel PC, Matthews RG, Schuman M, Sullivan PA. 1969. The production of superoxide anion radicals in the reaction of reduced flavins and flavoproteins with molecular oxygen. *Biochemical and Biophysical Research Communications* 36:891–897 DOI 10.1016/0006-291X(69)90287-3.
- Mattevi A. 2006. To be or not to be an oxidase: challenging the oxygen reactivity of flavoenzymes. *Trends in Biochemical Sciences* 31:276–283 DOI 10.1016/j.tibs.2006.03.003.
- Mennucci B, Tomasi J. 1997. Continuum solvation models: a new approach to the problem of solute's charge distribution and cavity boundaries. *Journal of Chemical Physics* 106:5151–5158 DOI 10.1063/1.473558.
- Mulliken RS. 1955. Electronic population analysis on LCAO-MO molecular wave functions I. *The Journal of Chemical Physics* 23:1833–1840 DOI 10.1063/1.1740588.
- Nakamura H. 1987. Semiclassical treatment of nonadiabatic transitions: multilevel curve crossing and nonadiabatic tunneling problems. *The Journal of Chemical Physics* 87:4031–4041 DOI 10.1063/1.452907.
- Pennati A, Gadda G. 2011. Stabilization of an intermediate in the oxidative half-reaction of human liver glycolate oxidase. *Biochemistry* 50:1–3 DOI 10.1021/bi101387w.
- Prabhakar R, Siegbahn PEM, Minaev BF, Ågren H. 2002. Activation of triplet dioxygen by glucose oxidase: spin-orbit coupling in the superoxide ion. *The Journal of Physical Chemistry B* 106:3742–3750 DOI 10.1021/jp014013q.
- Que L, Ho RYN. 1996. Dioxygen activation by enzymes with mononuclear non-heme iron active sites. *Chemical Reviews* 96:2607–2624 DOI 10.1021/cr960039f.
- Schmidt MW, Baldrige KK, Boatz JA, Elbert ST, Gordon MS, Jensen JH, Koseki S, Matsunaga N, Nguyen KA, Su S, Windus TL, Dupuis M, Montgomery JA. 1993. General atomic and molecular electronic structure system. *Journal of Computational Chemistry* 14:1347–1363 DOI 10.1002/jcc.540141112.
- Silva PJ. 2014. With or without light: comparing the reaction mechanism of dark-operative protochlorophyllide oxidoreductase with the energetic requirements of the light-dependent protochlorophyllide oxidoreductase. *PeerJ* 2:e551 DOI 10.7717/peerj.551.

- Silva PJ, Ramos MJ. 2007.** Reaction mechanism of the vitamin K-dependent glutamate carboxylase: a computational study. *The Journal of Physical Chemistry B* **111**:12883–12887 DOI [10.1021/jp0738208](https://doi.org/10.1021/jp0738208).
- Silva PJ, Ramos MJ. 2008.** A comparative density-functional study of the reaction mechanism of the O<sub>2</sub>-dependent coproporphyrinogen III oxidase. *Bioorganic & Medicinal Chemistry* **16**:2726–2733 DOI [10.1016/j.bmc.2008.01.008](https://doi.org/10.1016/j.bmc.2008.01.008).
- Silva PJ, Ramos MJ. 2009.** Computational studies on the reactivity of substituted 1,2-dihydro-1,2-azaborines. *The Journal of Organic Chemistry* **74**:6120–6129 DOI [10.1021/jo900980d](https://doi.org/10.1021/jo900980d).
- Sono M, Roach MP, Coulter ED, Dawson JH. 1996.** Heme-containing oxygenases. *Chemical Reviews* **96**:2841–2888 DOI [10.1021/cr9500500](https://doi.org/10.1021/cr9500500).
- Steiner RA, Janssen HJ, Roversi P, Oakley AJ, Fetzner S. 2010.** Structural basis for cofactor-independent dioxygenation of N-heteroaromatic compounds at the alpha/beta-hydrolase fold. *Proceedings of the National Academy of Sciences of the United States of America* **107**:657–662 DOI [10.1073/pnas.0909033107](https://doi.org/10.1073/pnas.0909033107).
- Thierbach S, Bui N, Zapp J, Chhabra SR, Kappl R, Fetzner S. 2014.** Substrate-assisted O<sub>2</sub> activation in a cofactor-independent dioxygenase. *Chemistry & Biology* **21**:217–225 DOI [10.1016/j.chembiol.2013.11.013](https://doi.org/10.1016/j.chembiol.2013.11.013).
- Tomasi J, Persico M. 1994.** Molecular interactions in solution: an overview of methods based on continuous distributions of the solvent. *Chemical Reviews* **94**:2027–2094 DOI [10.1021/cr00031a013](https://doi.org/10.1021/cr00031a013).
- Trott O, Olson AJ. 2010.** AutoDock Vina: improving the speed and accuracy of docking with a new scoring function, efficient optimization, and multithreading. *Journal of Computational Chemistry* **31**:455–461 DOI [10.1002/jcc.21334](https://doi.org/10.1002/jcc.21334).
- Visitsathawong S, Chenprakhon P, Chaiyen P, Surawatanawong P. 2015.** Mechanism of oxygen activation in a flavin-dependent monooxygenase: a nearly barrierless formation of C4a-hydroperoxyflavin via proton-coupled electron transfer. *Journal of the American Chemical Society* **137**:9363–9374 DOI [10.1021/jacs.5b04328](https://doi.org/10.1021/jacs.5b04328).
- Wallar BJ, Lipscomb JD. 1996.** Dioxygen activation by enzymes containing binuclear non-heme iron clusters. *Chemical Reviews* **96**:2625–2658 DOI [10.1021/cr9500489](https://doi.org/10.1021/cr9500489).
- White TA, Krishnan N, Becker DF, Tanner JJ. 2007.** Structure and kinetics of monofunctional proline dehydrogenase from *Thermus thermophilus*. *Journal of Biological Chemistry* **282**:14316–14327 DOI [10.1074/jbc.M700912200](https://doi.org/10.1074/jbc.M700912200).
- Wijaya IMM, Domratcheva T, Iwata T, Getzoff ED, Kandori H. 2016.** Single hydrogen bond donation from flavin N 5 to proximal asparagine ensures FAD reduction in DNA photolyase. *Journal of the American Chemical Society* **138**:4368–4376 DOI [10.1021/jacs.5b10533](https://doi.org/10.1021/jacs.5b10533).
- Yachandra VK, Sauer K, Klein MP. 1996.** Manganese cluster in photosynthesis: where plants oxidize water to dioxygen. *Chemical Reviews* **96**:2927–2950 DOI [10.1021/cr950052k](https://doi.org/10.1021/cr950052k).